








RESEARCH ARTICLE | SEPTEMBER 23 2024

# Magnetic domain study in $\text{Fe}_3\text{GaTe}_2$ ferromagnet with strong perpendicular anisotropy using magnetic force microscopy

Jungsub Lee ; Jinyoung Yun ; Yeonkyu Lee ; Beom Tak Kang; Jun Sung Kim; Nestor Haberkorn  ; Jeehoon Kim  *J. Appl. Phys.* 136, 123905 (2024)<https://doi.org/10.1063/5.0230813>View  
OnlineExport  
Citation

## Articles You May Be Interested In

Room-temperature unconventional topological Hall effect in a van der Waals ferromagnet  $\text{Fe}_3\text{GaTe}_2$ *APL Mater.* (January 2025)Room-temperature skyrmions in the van der Waals ferromagnet  $\text{Fe}_3\text{GaTe}_2$ *Appl. Phys. Lett.* (April 2024)Tremendous tunneling magnetoresistance effects based on van der Waals room-temperature ferromagnet  $\text{Fe}_3\text{GaTe}_2$  with highly spin-polarized Fermi surfaces*Appl. Phys. Lett.* (February 2023)

# Magnetic domain study in $\text{Fe}_3\text{GaTe}_2$ ferromagnet with strong perpendicular anisotropy using magnetic force microscopy

Cite as: J. Appl. Phys. **136**, 123905 (2024); doi: [10.1063/5.0230813](https://doi.org/10.1063/5.0230813)

Submitted: 26 July 2024 · Accepted: 5 September 2024 ·

Published Online: 23 September 2024



Jungsub Lee,<sup>1</sup> , Jinyoung Yun,<sup>1</sup> , Yeonkyu Lee,<sup>1</sup> , Beom Tak Kang,<sup>1</sup> Jun Sung Kim,<sup>1</sup> Nestor Haberkorn,<sup>1,2,3,a)</sup> and Jeehoon Kim<sup>1,a)</sup>

## AFFILIATIONS

<sup>1</sup>Department of Physics, Pohang University of Science and Technology, Pohang 37673, Republic of Korea

<sup>2</sup>Instituto Balseiro, Universidad Nacional de Cuyo and Comisión Nacional de Energía Atómica, Av. Bustillo 9500, 8400 San Carlos de Bariloche, Argentina

<sup>3</sup>Instituto de Nanociencia y Nanotecnología (CNEA - CONICET), Nodo Bariloche, Av. Bustillo 9500, 8400 San Carlos de Bariloche, Argentina

<sup>a)</sup>Authors to whom correspondence should be addressed: [nhaberk@cab.cnea.gov.ar](mailto:nhaberk@cab.cnea.gov.ar) and [jeehoon@postech.ac.kr](mailto:jeehoon@postech.ac.kr)

## ABSTRACT

We investigate the magnetic domain behavior of bulk  $\text{Fe}_3\text{GaTe}_2$ , a van der Waals (vdW) ferromagnet characterized by a Curie temperature ( $T_c$ ) of 350–380 K and significant perpendicular magnetic anisotropy (PMA). Using magnetic force microscopy, we present the evolution of magnetic domains during cooling from  $T_c$  to 300 K, and analyze magnetic domain images along the hysteresis loop at 4.2 K. Our observations reveal a strong temperature-dependent domain structure. From room temperature to  $T_c$ , we observe the coexistence of stripe, bubble, and surface spike domains. In contrast, in the zero-field cooled state at 4.2 K, irregular stripe and enclosed ring domains predominate. The correlation between global and local magnetization suggests that the hysteretic behavior in the magnetization results from the rapid nucleation of a few stripe domains evolving into intricate dendritic patterns, a phenomenon not previously observed in other vdW systems. These findings highlight the delicate balance among interlayer exchange coupling, thermal fluctuations, and PMA in the formation of various domains in a 3D vdW system, where shape anisotropy is minimized.

© 2024 Author(s). All article content, except where otherwise noted, is licensed under a Creative Commons Attribution (CC BY) license (<https://creativecommons.org/licenses/by/4.0/>). <https://doi.org/10.1063/5.0230813>

## I. INTRODUCTION

Finding a van der Waals ferromagnet (vdW FM) that operates at room temperature (RT) has been a significant challenge in the study of magnetism, especially in the field of spintronics.<sup>1–3</sup> According to the Wagner–Mermin theory, 2D ferromagnets were believed to be non-existent due to thermal fluctuations destroying long-range magnetic order.<sup>4</sup> However, certain vdW systems have shown intrinsic ferromagnetism in flakes consisting of a few layers, attributed to the presence of a spin-wave excitation gap.<sup>5–7</sup> Examples include  $\text{CrI}_3$  with  $T_c \approx 45$  K,<sup>8</sup>  $\text{Cr}_2\text{Ge}_2\text{Te}_6$  with  $T_c \approx 65$  K,<sup>9</sup>  $\text{Fe}_3\text{GeTe}_2$  with  $T_c \approx 230$  K,<sup>10</sup>  $\text{Fe}_4\text{GeTe}_2$  with  $T_c \approx 270$  K,<sup>11</sup> and  $\text{Fe}_{5-x}\text{GeTe}_2$  with  $T_c$  slightly higher than RT.<sup>12</sup> Considering that most systems exhibit ferromagnetic (FM) order below RT and that

thermal fluctuations suppress intrinsic magnetic order in the 2D limit, stabilizing magnetism at high temperatures initially appeared to be a significant challenge. Strategies have included the design of ionic liquid gates (e.g., Li-doped  $\text{Fe}_3\text{GeTe}_2$ )<sup>13</sup> and heterostructures combining other ferromagnetic systems.<sup>14</sup> However, this goal has recently been achieved in  $\text{Fe}_3\text{GaTe}_2$  (FGaT),<sup>15,16</sup> a vdW FM with robust perpendicular magnetic anisotropy (PMA) and a  $T_c$  higher than RT (350–380 K).

The application of vdW FMs typically involves thin flakes that can be utilized in various technologies based on their electrical and magnetic properties, encompassing metallic, superconducting, and insulating systems with ferromagnetic (FM) and antiferromagnetic (AFM) order.<sup>2</sup> Moreover, vdW FMs are particularly intriguing in

25 June 2025 10:39:19

systems exhibiting strong PMA, which influences domain patterns. As the thickness decreases to a few unit cells, it becomes feasible to stabilize domain morphologies such as bubbles and skyrmions.<sup>17–20</sup> These structures often manifest in the maximum cooled state or under small fields near  $T_c$ , making them highly appealing for memory storage applications,<sup>21</sup> arising from the intricate balance between magnetocrystalline and shape anisotropies.

Conversely, in 3D-limit vdW systems where shape anisotropy is minimized, domain structures tend to vary significantly with temperature and external fields, resulting in a diverse array of shapes.<sup>22–25</sup> Thick vdW crystals such as  $\text{Fe}_3\text{GeTe}_2$ ,  $\text{CrGeTe}_3$ , and  $\text{Fe}_4\text{GeTe}_2$  have exhibited structures including labyrinth, enclosed ring, and combination of stripe domain (SD), bubble domain (BD), and spike-like domain (SLD). Exploring domains in vdW systems while mitigating the impact of shape anisotropy provides insight into the behavior of other systems such as soft and hard magnets.<sup>22,26,27</sup> Additionally, the correlation between magnetic domains and anomalous transport properties<sup>28,29</sup> is significant, as the Hall resistivity  $\rho_{xy}$  scales with changes in magnetization, thus reflecting the evolution of magnetic domains.<sup>30,31</sup>

In this study, we investigate a variety of magnetic domains in a vdW FGaT single crystal from 4.25 K to above RT using magnetic force microscopy (MFM). The vdW FGaT, with its hexagonal structure (space group  $P63/mmc$ ),<sup>15</sup> boasts a record-high  $T_c$  of 350–380 K among known layered vdW FMs, making it suitable for device design spanning cryogenic to RT. This facilitates the research of domain structures over a broad temperature range and their susceptibility to thermal fluctuations. While previous studies have shown that thin flakes of FGaT exhibit stabilized skyrmion structures even at RT,<sup>18–20</sup> our study focuses on the behavior of magnetic domains in the bulk regime across a wide range of temperatures, arising from the competition among thermal fluctuations, interlayer coupling strength, and uniaxial anisotropy.

## II. EXPERIMENTAL

FGaT single crystals were grown using chemical vapor transport (CVT). High-purity powders of Fe, Ga, and Te were mixed in a mole ratio of 3:1:2 and placed into a quartz ampoule. Iodine was used as the transport agent. The synthesis was carried out in a 2-zone furnace, with the hot zone set to 750 °C and the cold zone set to 700 °C, creating a temperature gradient of 5 °C/cm. The sample was heated for 7 days to complete the synthesis. Scanning electron microscopy (SEM) and energy dispersive x-ray spectroscopy (EDS) were performed using an FE-SEM (JSM 7800F Prime) to determine the elemental composition of the crystal. Magnetization measurements were carried out using a physical property measurement system (PPMS, Quantum Design). Hall measurements were performed using an Oxford 12 T Dewar (Oxford Instruments).

MFM images above RT were obtained with an Nx10 (Park Systems) using phase mapping in the amplitude modulation (AM) mode. The experiments were conducted by adjusting the temperature with a heating sample holder module. To minimize thermal drift, the experiments were conducted by raising the temperature and then allowing sufficient time for stabilization before proceeding with imaging. MFM images at low temperatures were acquired

using home-built cryogenic equipment in conjunction with a 2-2-9 T vector magnet, allowing magnetic field manipulation along the x, y, and z axes.<sup>32</sup> The magnetic contrast in MFM images is determined by the frequency shift ( $\Delta f$ ) of the cantilever. The coercive field of the tip at 4.3 K is approximately 800 G for the out-of-plane direction. Both systems used PPP-MFMR (Nanosensor) cantilevers with a resonance frequency of 75 kHz.

## III. RESULT AND DISCUSSION

### A. Characterization of the material and magnetization and Hall measurement

Figures 1(a) and 1(b) show the SEM images of the crystal used in this study after cleaving. The sample displays a plate-like structure with well-defined terraces, characteristic of layered compounds. Figures 1(c)–1(e) present the EDS analysis of the crystal surface, confirming the uniform distribution of Fe(47 at. %), Ga(18 at. %), and Te(33 at. %) elements. Both defect-free surface morphology and homogeneous chemical composition are suitable for investigating the domain patterns.

Before studying the magnetic domains, we first characterized the magnetic properties and magneto-transport characteristics of the bulk FGaT single crystal. The temperature-dependent magnetization of the FGaT bulk sample was measured from 2 to 400 K at 0.1 T, as shown in Fig. 2(a). The field-dependent magnetization was measured at 2 K from  $-0.7$  to  $0.7$  T, as shown in Fig. 2(b). While the evolution of the magnetization under an applied field is smooth for  $\mathbf{H} \parallel ab$ , a hysteretic signal characteristic of soft ferromagnetism was observed for  $\mathbf{H} \parallel c$ . Similar data behavior and the presence of PMA were reported previously.<sup>15</sup> The saturation field with  $\mathbf{H} \parallel ab$  is expected above 6 T, whereas for  $\mathbf{H} \parallel c$ , saturation is reached close to 0.6 T, with a saturation magnetization of approximately 68 emu/g. Moreover, the  $\mathbf{H} \parallel c$  curve displays a small remanence and a coercive field close to 0.1 T. The inset shows the Hall

25 June 2025 10:39:19

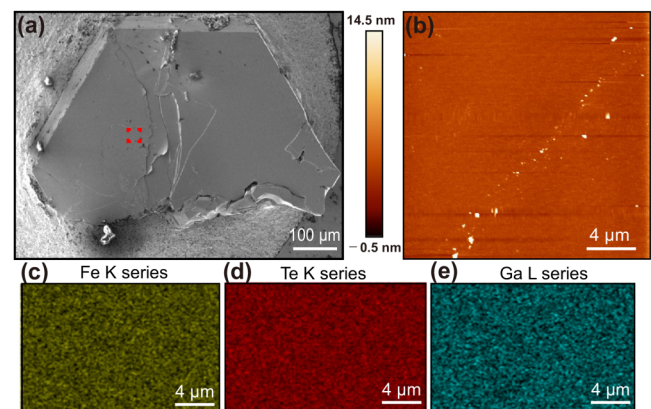


**FIG. 1.** Characterization of the FGaT sample. (a) SEM image of the cleaved single crystal of FGaT. The hatched rectangular box indicates the region where the EDS image was obtained. (b) AFM topographic image of FGaT with a scan size of  $20 \times 20 \mu\text{m}^2$ . (c)–(e) EDS images of Fe-K, Ga-L, and Te-L, respectively.

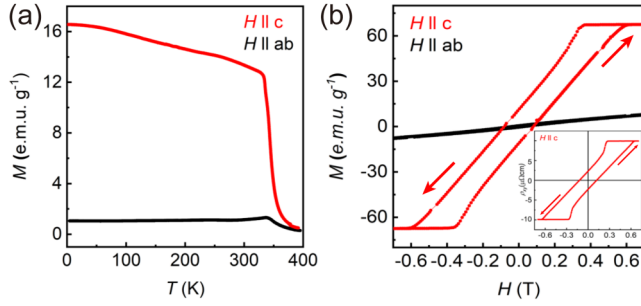


**FIG. 2.** (a) Temperature dependence of the magnetization curve with the field applied parallel to the  $c$ -axis ( $\mathbf{H} \parallel c$ ) and to the  $ab$  plane ( $\mathbf{H} \parallel ab$ ). (b) Field-dependent magnetization applied parallel to the  $\mathbf{H} \parallel c$  and the  $\mathbf{H} \parallel ab$  plane at 2 K. The inset shows the field-dependent Hall resistance applied magnetic field parallel to the  $c$ -axis at 2 K.

measurement with  $\mathbf{H} \parallel c$  between  $-0.7$  and  $0.7$  T at 2 K. No special features are observed for larger negative and positive fields. The Hall signal displays an anomalous contribution that follows the magnetization hysteresis loop displayed in Fig. 2(b), indicating the expected correlation between the out-of-plane changes in the magnetization.<sup>30</sup>

### B. Temperature-dependent magnetic domains around $T_c$

To observe the local evolution of domains at  $T_c$ , we conducted MFM experiments, capturing images from 358 K to RT.

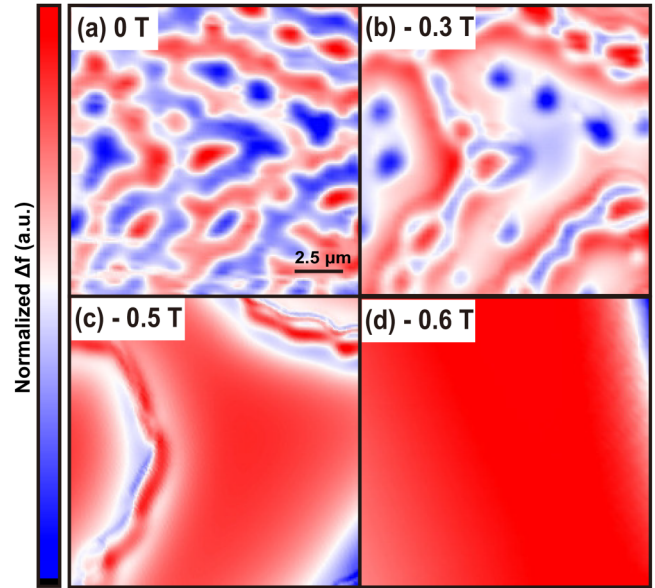


**FIG. 4.** MFM images at  $T = 4.25$  K from the zero-field cooled state to  $\mu_0 H = -0.6$  T. The size of all images is  $15 \times 15 \mu\text{m}^2$ , and the tip-lift height is 100 nm. All images are normalized to a frequency shift range of 50 to  $-50$  Hz.

Figures 3(a)–3(d) present a summary of these MFM images. The images indicate that as magnetic order appears, the domains consist of a combination of SD and BD, with their intensity and shapes systematically changing as the temperature decreases to RT. The initial

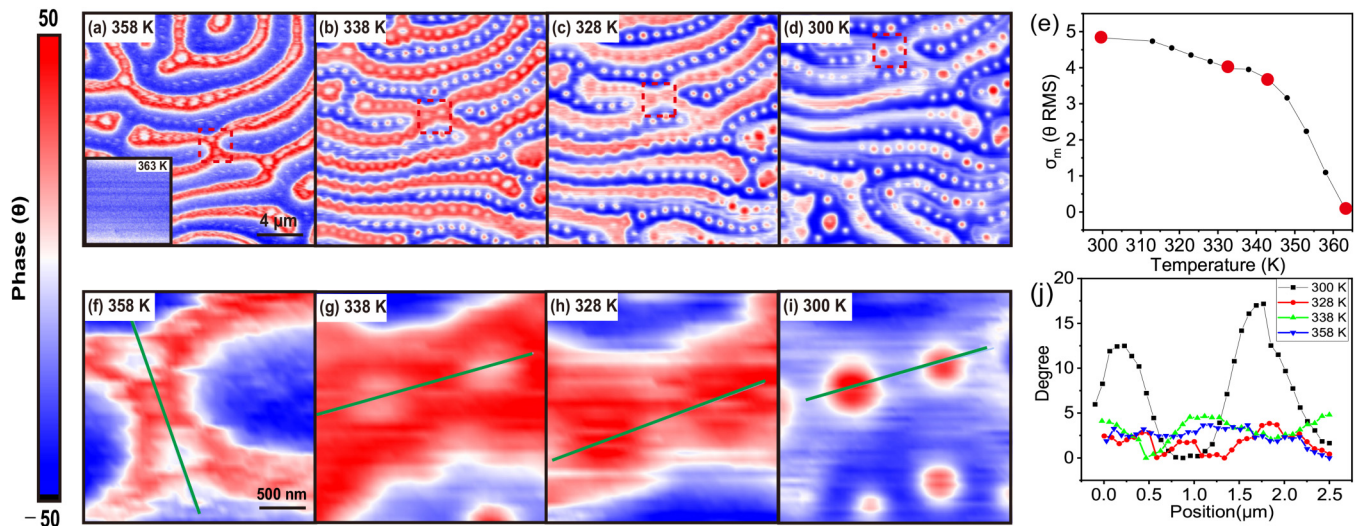


**FIG. 3.** (a)–(d) MFM images were obtained while cooling the sample from 358 K to RT. The inset in (a) shows an image obtained after the phase transition at 363 K. (e) The root mean square of the phase as a function of temperature is shown, with the red dots corresponding to data obtained from (a) to (d). The black dots were obtained from temperature-dependent images that are not displayed. The hatched square box in (a) to (d) is magnified and displayed in (f) to (i), with a size of  $2.5 \times 2.5 \mu\text{m}^2$ . The profiles along the green lines in (f) to (i) are plotted in (j). The images are normalized to represent relative phase values from  $50^\circ$  to  $-50^\circ$ . Image sizes are  $20 \times 20 \mu\text{m}^2$ , with a tip-lift height of 200 nm.

25 June 2025 10:39:19



appearance of domains near  $T_c$ , featuring SD and BD, is similar to those previously observed in  $\text{Fe}_3\text{GeTe}_2$  at low temperatures.<sup>22</sup> The morphology can be described as a coexistence of SD and SLD, which seem to minimize surface magnetic energies as crystalline anisotropy becomes dominant. For FGaT, SLD initially appears between and within the SDs. However, as the temperature approaches RT, the

intensity change of the SLDs residing inside the SDs is more significant than that of the SLDs between the SDs.

Figure 3(e) shows the root mean square of phase as a function of temperature obtained from Figs. 3(a)–3(d). This curve agrees well with the  $M$ – $T$  curve for  $\mathbf{H} \parallel c$ , as shown in Fig. 2(a). To investigate the transformation from SDs to bubble like domains (BLDs),

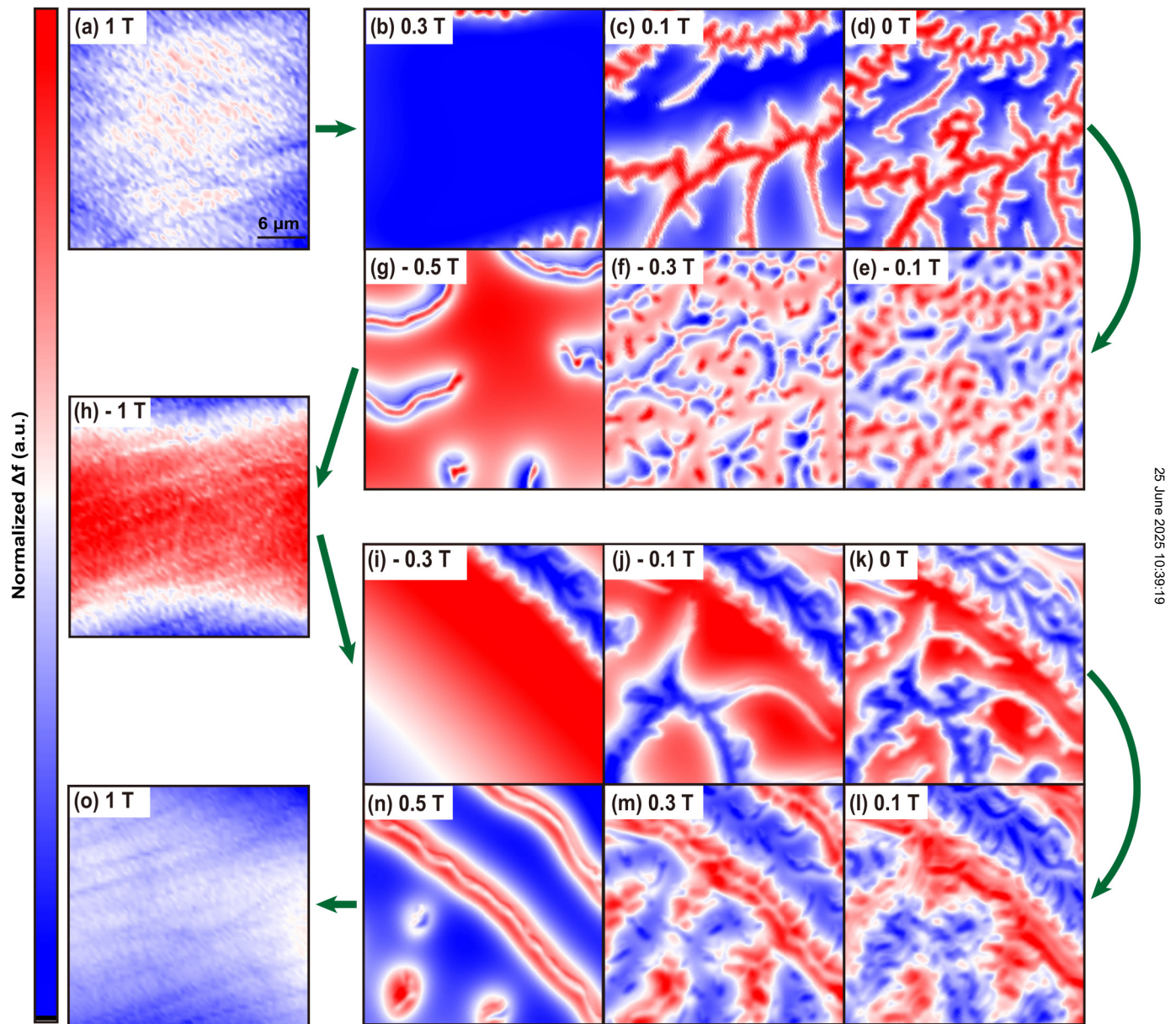


**FIG. 5.** MFM images showing the evolution of magnetic domains in response to a magnetic field parallel to the  $c$ -axis. (a)–(h) The magnetic domain images obtained by applying an external magnetic field from 1 to  $-1$  T. (h)–(o) The evolution of magnetic domains as the magnetic field is applied from  $-1$  to 1 T. The size of all images is  $30 \times 30 \mu\text{m}^2$ , and the tip-lift height is 200 nm. All images are normalized to a frequency shift range of 50 to  $-50$  Hz, excluding (a), (h), and (o). (a), (h), and (o) have a range of 0.5 to  $-0.5$  Hz.

25 June 2025 10:39:19

we focus on the evolution of the SLDs shown in the dotted red box in Figs. 3(a)–3(d), with the corresponding zoom-in views shown in Figs. 3(f)–3(i). The two SLDs at 358 K change their positions as the temperature decreases to 338 K and disappear at 328 K, leaving the SD alone. The remaining SD then breaks into BLDs at 300 K. The changes in the profiles, indicated by green lines in each image, are summarized in Fig. 3(j), where the collapse of the SLD and the transformation of SD into the BLD are observed.

### C. Field-dependent magnetic domain evolution from the zero-field cooled state

Next, we analyze the magnetic domain structure and its evolution under a magnetic field at 4.2 K. In addition to investigating domain structures and comparing them with other systems having different PMA and lower  $T_c$ , this study is relevant for the design of superconducting/FM hybrids in applications where a reduction in the thickness is not required. The data presentation is divided into two sets. First, we show the MFM images of the magnetic evolution from the zero-field cooled state to saturation with  $\mathbf{H} \parallel c$ . Second, we present corresponding images in the hysteresis loop with  $\mathbf{H} \parallel c$ , similar to Fig. 2(b). For these measurements, MFM images were acquired using frequency modulation. In this mode, the frequency shift of the cantilever caused by the magnetic force due to the magnetic moment of FGaT can be expressed as  $\Delta f = -\frac{f_0}{2k} \frac{\partial F}{\partial z}$ . To prevent the images from becoming blurry due to the gradual decrease in the frequency shift of the domains, the maximum and minimum values of the frequency shift were normalized to  $\pm 50$  Hz, clearly showing the relative domain changes among the images.

Figures 4(a)–4(d) present the magnetic domains at  $T = 4.2$  K, with the magnetic field intensity increasing from the zero-field cooled state to  $-0.6$  T. The magnetic structures at the zero-field cooled state at 4.2 K differ from those observed at RT, as compared between Figs. 3(d) and 4(a). Unlike at RT, the image at 4.2 K displays the regions with magnetization in both upward and downward directions, showing interconnected SD and irregular enclosed domains with domain widths ranging between 1 and  $2 \mu\text{m}$ . As the magnetic field approaches saturation, the domain walls grow in width, aligning themselves with the increasing field, which is evident in Figs. 4(b) and 4(c). At intermediate fields, large regions of downward magnetization coexist with well-defined BDs. These features contrast with observations in systems such as  $\text{Fe}_3\text{GeTe}_2$  and  $\text{Fe}_4\text{GeTe}_2$  with weaker PMA,<sup>22,25</sup> where SDs and BDs coexist with SLD, minimizing magnetic energy within wide SDs.

### D. The evolution of magnetic domains along the full hysteresis loop

Figure 5 displays the MFM images obtained along the hysteresis loop at  $T = 4.25$  K, where the field starts from 1 T and sequentially decreases to  $-1$  T and then returns to 1 T. The hysteresis loop in FGaT, shown in Fig. 2(b), differs from the square shape with large coercivity seen in hard magnets. As the magnetic field decreases from saturation and reaches around 0.3 T, the nucleation of irregular SD is observed, consistent with the rapid drop in magnetization in the loop. A smoother reduction of magnetization

occurs through the dendritic ramification of the initial domains rather than the appearance of new ones as the field decreases to zero. When the field is further decreased in the opposite direction, the saturation state is achieved through the gradual recombination of the dendritic domains (DDs), as shown in Figs. 5(e) and 5(f). Upon changing the field along the other side of the hysteresis loop, from  $-1$  to 1 T, the MFM images display features similar to those observed from 1 to  $-1$  T. From these images, the following features are noted: (1) the rapid drop in magnetization as the field decreases from saturation is caused by the nucleation of a small number of SDs—two SDs in the  $30 \times 30 \mu\text{m}^2$  field of view—which later evolve into DDs as a mechanism to reduce magnetization; (2) the features of the DDs in this material with strong PMA are different from systems showing the coexistence of SD and BD<sup>17,22,24,25</sup> with moderate PMA. It should be noted that the branching and expansion of initial domains, rather than the creation of new ones, are possibly related to the observed anomalous Hall effect displayed in Fig. 2(b). Following the nucleation of a few SDs, the DDs facilitate a smooth transition in magnetization,<sup>33</sup> resulting in an anomalous Hall response to varying magnetic fields.

### IV. SUMMARY

Our results underscore the intricate interplay between thermal fluctuations and interlayer coupling in vdW single crystals exhibiting strong PMA. Magnetic domain structures show the pronounced variations between RT and low temperatures. At RT, BDs, SDs, and SLDs coexist at micron scales, although many of these features diminish as the temperature decreases. Upon zero-field cooling, the magnetic domains exhibit interconnected SDs and irregular enclosed domains. Upon saturation, the domain structure demonstrates the rapid propagation of a few SDs that gradually evolve into DDs, which possibly give rise to the anomalous Hall effect, highlighting the connection between the shape of magnetic domains and electrical transport in van der Waals ferromagnetic materials.

Additionally, the domain structures observed in this study differ from those reported in other thick vdW systems with weaker PMA, where a coexistence of SDs, BDs, and SLDs occurs at the microscale.<sup>17,22,24,25</sup> In this system with strong PMA, recognized for its potential to stabilize skyrmion-like structures in thin flakes,<sup>16</sup> the significant differences in domain structures between RT and low temperatures suggest a complex competition among thermal fluctuations, uniaxial anisotropies, and interlayer coupling. Further investigations are crucial to fully comprehend the implications of these findings for spintronics and magnetic device applications across different operating temperatures.

### ACKNOWLEDGMENTS

This work was supported by Basic Science Research Program through the National Research Foundation of Korea (NRF) funded by the Ministry of Science, and ICT and Future Planning (Nos. NRF-2019R1A2C2090356, RS-2024-00410027, RS-2023-00222408, and NRF-2022H1D3A3A01077468f); and the Technology Development Program (Grant No. S3198743) funded by the Ministry of SMEs and Startups (MSS, Korea).

25 June 2025 10:39:19

## AUTHOR DECLARATIONS

## Conflict of Interest

The authors have no conflicts to disclose.

## Author Contributions

J.L., J.Y., and Y.L. contributed equally to this paper.

**Jungsub Lee:** Formal analysis (equal); Investigation (equal); Methodology (equal); Software (equal); Validation (equal); Visualization (equal); Writing – original draft (equal); Writing – review & editing (equal). **Jinyoung Yun:** Investigation (equal); Methodology (equal); Software (equal); Validation (equal); Visualization (equal); Writing – original draft (equal); Writing – review & editing (equal). **Yeonkyu Lee:** Investigation (equal); Methodology (equal); Software (equal); Validation (equal); Visualization (equal); Writing – original draft (equal); Writing – review & editing (equal). **Beom Tak Kang:** Investigation (equal); Methodology (equal); Validation (equal); Writing – original draft (equal). **Beom Tak Kang:** Methodology (equal); Supervision (equal); Validation (equal); Writing – original draft (equal). **Nestor Haberkorn:** Conceptualization (equal); Investigation (equal); Methodology (equal); Validation (equal); Writing – original draft (equal). **Jecheon Kim:** Conceptualization (equal); Data curation (equal); Formal analysis (equal); Funding acquisition (equal); Methodology (equal); Supervision (equal); Validation (equal); Writing – original draft (equal); Writing – review & editing (equal).

## DATA AVAILABILITY

The data that support the findings of this study are available within the article.

## REFERENCES

- <sup>1</sup>S. Yang, T. Zhang, and C. Jiang, “van der Waals magnets: Material family, detection and modulation of magnetism, and perspective in spintronics,” *Adv. Sci.* **8**, 2002488 (2021).
- <sup>2</sup>H. Kurebayashi, J. H. Garcia, S. Khan, J. Sinova, and S. Roche, “Magnetism, symmetry and spin transport in van der Waals layered systems,” *Nat. Rev. Phys.* **4**, 150–166 (2022).
- <sup>3</sup>X. Jiang, Q. Liu, J. Xing, N. Liu, Y. Guo, Z. Liu, and J. Zhao, “Recent progress on 2D magnets: Fundamental mechanism, structural design and modification,” *Appl. Phys. Rev.* **8**, 031305 (2021).
- <sup>4</sup>N. D. Mermin and H. Wagner, “Absence of ferromagnetism or antiferromagnetism in one- or two-dimensional isotropic Heisenberg models,” *Phys. Rev. Lett.* **17**, 1133–1136 (1966).
- <sup>5</sup>C. Gong, L. Li, Z. Li *et al.*, “Discovery of intrinsic ferromagnetism in two-dimensional van der Waals crystals,” *Nature* **546**, 265–269 (2017).
- <sup>6</sup>Z. Li, T. Cao, and S. G. Louie, “Two-dimensional ferromagnetism in few-layer van der Waals crystals: Renormalized spin-wave theory and calculations,” *J. Magn. Magn. Mater.* **463**, 28–35 (2018).
- <sup>7</sup>S. Jenkins, L. Rózsa, U. Atxitia *et al.*, “Breaking through the Mermin-Wagner limit in 2D van der Waals magnets,” *Nat. Commun.* **13**, 6917 (2022).
- <sup>8</sup>B. Huang, G. Clark, E. Navarro-Moratalla *et al.*, “Layer-dependent ferromagnetism in a van der Waals crystal down to the monolayer limit,” *Nature* **546**, 270–273 (2017).
- <sup>9</sup>W. Z. Zhuo *et al.*, “Manipulating ferromagnetism in few-layered  $\text{Cr}_2\text{Ge}_2\text{Te}_6$ ,” *Adv. Mater.* **33**, 2008586 (2021).
- <sup>10</sup>Z. Fei, B. Huang, P. Malinowski *et al.*, “Two-dimensional itinerant ferromagnetism in atomically thin  $\text{Fe}_3\text{GeTe}_2$ ,” *Nat. Mater.* **17**, 778–782 (2018).
- <sup>11</sup>J. Seo *et al.*, “Nearly room temperature ferromagnetism in a magnetic metal-rich van der Waals metal,” *Sci. Adv.* **6**, eaay8912 (2020).
- <sup>12</sup>H. Zhang *et al.*, “Itinerant ferromagnetism in van der Waals  $\text{Fe}_{5-x}\text{GeTe}_2$  crystals above room temperature,” *Phys. Rev. B* **102**, 064417 (2020).
- <sup>13</sup>Y. Deng, Y. Yu, Y. Song *et al.*, “Gate-tunable room-temperature ferromagnetism in two-dimensional  $\text{Fe}_3\text{GeTe}_2$ ,” *Nature* **563**, 94–99 (2018).
- <sup>14</sup>M. Yang, Q. Li, R. V. Chopdekar *et al.*, “Creation of skyrmions in van der Waals ferromagnet  $\text{Fe}_3\text{GeTe}_2$  on  $(\text{Co/Pd})_n$  superlattice,” *Sci. Adv.* **6**, eaab5157 (2020).
- <sup>15</sup>G. Zhang, F. Guo, H. Wu *et al.*, “Above-room-temperature strong intrinsic ferromagnetism in 2D van der Waals  $\text{Fe}_3\text{GaTe}_2$  with large perpendicular magnetic anisotropy,” *Nat. Commun.* **13**, 5067 (2022).
- <sup>16</sup>M. Wang, B. Lei, K. Zhu *et al.*, “Hard ferromagnetism in van der Waals  $\text{Fe}_3\text{GaTe}_2$  nanoflake down to monolayer,” *npj 2D Mater. Appl.* **8**, 22 (2024).
- <sup>17</sup>R. Fujita, P. Bassirian, Z. Li *et al.*, “Layer-dependent magnetic domains in atomically thin  $\text{Fe}_3\text{GeTe}_2$ ,” *ACS Nano* **16**, 10545–10553 (2022).
- <sup>18</sup>X. Hou *et al.*, “Room-temperature skyrmions in the van der Waals ferromagnet  $\text{Fe}_3\text{GaTe}_2$ ,” *Appl. Phys. Lett.* **124**, 142404 (2024).
- <sup>19</sup>Z. Li, H. Zhang, G. Li *et al.*, “Room-temperature sub-100 nm Néel-type skyrmions in non-stoichiometric van der Waals ferromagnet  $\text{Fe}_{3-x}\text{GaTe}_2$  with ultrafast laser writability,” *Nat. Commun.* **15**, 1017 (2024).
- <sup>20</sup>C. Liu, S. Zhang, H. Hao, H. Algaidi, Y. Ma, and X.-X. Zhang, “Magnetic skyrmions above room temperature in a van der Waals ferromagnet  $\text{Fe}_3\text{GaTe}_2$ ,” *Adv. Mater.* **36**, 2311022 (2024).
- <sup>21</sup>R. Tomasello, E. Martinez, R. Zivieri *et al.*, “A strategy for the design of skyrmion racetrack memories,” *Sci. Rep.* **4**, 6784 (2014).
- <sup>22</sup>N. León-Brito *et al.*, “Magnetic microstructure and magnetic properties of uniaxial itinerant ferromagnet  $\text{Fe}_3\text{GeTe}_2$ ,” *J. Appl. Phys.* **120**, 083903 (2016).
- <sup>23</sup>S. Grebenchuk, E. J. G. Santos, M. Koperski *et al.*, “Topological spin textures in an insulating van der Waals ferromagnet,” *Adv. Mater.* **36**, 2311949 (2024).
- <sup>24</sup>Y. Lee, J. Yun, G. Kim *et al.*, “The magnetic states of a van der Waals ferromagnet  $\text{CrGeTe}_3$  probed by vector-field magnetic force microscopy,” *Appl. Phys. Lett.* **124**, 130601 (2024).
- <sup>25</sup>J. Yun, Y. Lee, G. Kim *et al.*, “Probing local magnetic states in the van der Waals ferromagnet  $\text{Fe}_4\text{GeTe}_2$  by a vector-field magnetic force microscope,” *J. Mater. Sci.* **59**, 6415–6424 (2024).
- <sup>26</sup>E. Zueco, W. Rave, R. Schäfer, A. Hubert, and L. Schultz, “Combined Kerr-/magnetic force microscopy on  $\text{NdFeB}$  crystals of different crystallographic orientation,” *J. Magn. Magn. Mater.* **190**, 42–47 (1998).
- <sup>27</sup>N. Volker, V. Silvia, S. Tina, and S. Ludwig, “Epitaxial hard magnetic  $\text{SmCo}_5$  MFM tips—A new approach to advanced magnetic force microscopy imaging,” *Nanoscale* **10**, 16881–16886 (2018).
- <sup>28</sup>M. Lohmann, T. Su, B. Niu *et al.*, “Probing magnetism in insulating  $\text{Cr}_2\text{Ge}_2\text{Te}_6$  by induced anomalous Hall effect in Pt,” *Nano Lett.* **19**, 2397–2403 (2019).
- <sup>29</sup>R. R. Chowdhury, S. DuttaGupta, C. Patra *et al.*, “Unconventional Hall effect and its variation with Co-doping in van der Waals  $\text{Fe}_3\text{GeTe}_2$ ,” *Sci. Rep.* **11**, 14121 (2021).
- <sup>30</sup>Y. Deng *et al.*, “Layer-number-dependent magnetism and anomalous Hall effect in van der Waals ferromagnet  $\text{Fe}_5\text{GeTe}_2$ ,” *Nano Lett.* **22**, 9839–9846 (2022).
- <sup>31</sup>M. Huang *et al.*, “Colossal anomalous Hall effect in ferromagnetic van der Waals  $\text{CrTe}_2$ ,” *ACS Nano* **15**, 9759–9763 (2021).
- <sup>32</sup>G. Kim, J. Yun, Y. Lee, and J. Kim, “Construction of a vector-field cryogenic magnetic force microscope,” *Rev. Sci. Instrum.* **93**, 063701 (2022).
- <sup>33</sup>A. Hubert and R. Schäfer, *Magnetic Domains: The Analysis of Magnetic Microstructures* (Springer-Verlag, Berlin, 1998).

25 June 2025 10:39:19